Ultrathin platelet antennas mediated light-matter interaction in monolayer MoS₂

YINGYI YANG,[1] DI WANG,[2] ZHENG JIE TAN,[1] XIANG XIONG,[2,3] MU WANG,[2] RUWEN PENG,[2] AND NICHOLAS X. FANG[1,4]

[1]*Department of Mechanical Engineering, Massachusetts Institute of Technology, Cambridge, Massachusetts 02139, USA*
[2]*National Laboratory of Solid State Microstructures and School of Physics, and Collaborative Innovation Center of Advanced Microstructures, Nanjing University, Nanjing 210093, China*
[3]*xiang@nju.edu.cn*
[4]*nicfang@mit.edu*

Abstract: Monolayer MoS₂ is an emerging two-dimensional semiconductor that has seen wide applications in optoelectronic and light-emitting devices. Here we report on the antenna-enhanced spontaneous emission of monolayer MoS₂, which has weak absorbance and low intrinsic quantum yield. The ultrathin silver platelet antennas we use can both increase the absorption cross-section and improve the transmission efficiency via controlling the optical field at nanometer scale. Experimental results indicate the photoluminescence enhancement can reach 4 times, which is also supported by numerical analysis of both excitation and emission processes with respect to the thickness of spacer layer. This ultrathin structure can facilitate the development of on-chip emitters and valley-based devices, especially in cases of large area sample or flexible substrate.

References and links

1. S. Z. Butler, S. M. Hollen, L. Cao, Y. Cui, J. A. Gupta, H. R. Gutiérrez, T. F. Heinz, S. S. Hong, J. Huang, A. F. Ismach, E. Johnston-Halperin, M. Kuno, V. V. Plashnitsa, R. D. Robinson, R. S. Ruoff, S. Salahuddin, J. Shan, L. Shi, M. G. Spencer, M. Terrones, W. Windl, and J. E. Goldberger, "Progress, Challenges, and Opportunities in Two-Dimensional Materials Beyond Graphene," ACS Nano **7**(4), 2898–2926 (2013).
2. Q. H. Wang, K. Kalantar-Zadeh, A. Kis, J. N. Coleman, and M. S. Strano, "Electronics and optoelectronics of two-dimensional transition metal dichalcogenides," Nat. Nanotechnol. **7**(11), 699–712 (2012).
3. K. S. Novoselov, D. Jiang, F. Schedin, T. J. Booth, V. V. Khotkevich, S. V. Morozov, and A. K. Geim, "Two-dimensional atomic crystals," Proc. Natl. Acad. Sci. U.S.A. **102**(30), 10451–10453 (2005).
4. A. Kuc, N. Zibouche, and T. Heine, "Influence of quantum confinement on the electronic structure of the transition metal sulfide TS₂," Phys. Rev. B **83**(24), 245213 (2011).
5. B. Radisavljevic, A. Radenovic, J. Brivio, V. Giacometti, and A. Kis, "Single-layer MoS₂ transistors," Nat. Nanotechnol. **6**(3), 147–150 (2011).
6. G. A. Salvatore, N. Münzenrieder, C. Barraud, L. Petti, C. Zysset, L. Büthe, K. Ensslin, and G. Tröster, "Fabrication and transfer of flexible few-layers MoS₂ thin film transistors to any arbitrary substrate," ACS Nano **7**(10), 8809–8815 (2013).
7. H. S. Lee, S. W. Min, Y. G. Chang, M. K. Park, T. Nam, H. Kim, J. H. Kim, S. Ryu, and S. Im, "MoS₂ nanosheet phototransistors with thickness-modulated optical energy gap," Nano Lett. **12**(7), 3695–3700 (2012).
8. D. J. Late, Y. K. Huang, B. Liu, J. Acharya, S. N. Shirodkar, J. Luo, A. Yan, D. Charles, U. V. Waghmare, V. P. Dravid, and C. N. R. Rao, "Sensing behavior of atomically thin-layered MoS₂ transistors," ACS Nano **7**(6), 4879–4891 (2013).
9. O. Lopez-Sanchez, D. Lembke, M. Kayci, A. Radenovic, and A. Kis, "Ultrasensitive photodetectors based on monolayer MoS₂," Nat. Nanotechnol. **8**(7), 497–501 (2013).
10. Z. Y. Zhu, Y. C. Cheng, and U. Schwingenschlögl, "Giant spin-orbit-induced spin splitting in two-dimensional transition-metal dichalcogenide semiconductors," Phys. Rev. B **84**(15), 153402 (2011).
11. K. F. Mak, K. L. McGill, J. Park, and P. L. McEuen, "The valley Hall effect in MoS2 transistors," Science **344**(6191), 1489–1492 (2014).
12. G. Eda and S. A. Maier, "Two-dimensional crystals: managing light for optoelectronics," ACS Nano **7**(7), 5660–5665 (2013).

13. K. F. Mak, C. Lee, J. Hone, J. Shan, and T. F. Heinz, "Atomically thin MoS$_2$: a new direct-gap semiconductor," Phys. Rev. Lett. **105**(13), 136805 (2010).
14. P. P. Pompa, L. Martiradonna, A. D. Torre, F. D. Sala, L. Manna, M. De Vittorio, F. Calabi, R. Cingolani, and R. Rinaldi, "Metal-enhanced fluorescence of colloidal nanocrystals with nanoscale control," Nat. Nanotechnol. **1**(2), 126–130 (2006).
15. A. Kinkhabwala, Z. Yu, S. Fan, Y. Avlasevich, K. Müllen, and W. E. Moerner, "Large single-molecule fluorescence enhancements produced by a bowtie nanoantenna," Nat. Photonics **3**(11), 654–657 (2009).
16. G. M. Akselrod, C. Argyropoulos, T. B. Hoang, C. Ciracì, C. Fang, J. Huang, D. R. Smith, and M. H. Mikkelsen, "Probing the mechanisms of large Purcell enhancement in plasmonic nanoantennas," Nat. Photonics **8**(11), 835–840 (2014).
17. A. Rose, T. B. Hoang, F. McGuire, J. J. Mock, C. Ciracì, D. R. Smith, and M. H. Mikkelsen, "Control of radiative processes using tunable plasmonic nanopatch antennas," Nano Lett. **14**(8), 4797–4802 (2014).
18. L. Novotny and N. van Hulst, "Antennas for light," Nat. Photonics **5**(2), 83–90 (2011).
19. S. Najmaei, A. Mlayah, A. Arbouet, C. Girard, J. Léotin, and J. Lou, "Plasmonic pumping of excitonic photoluminescence in hybrid MoS$_2$-Au nanostructures," ACS Nano **8**(12), 12682–12689 (2014).
20. S. Butun, S. Tongay, and K. Aydin, "Enhanced light emission from large-area monolayer MoS$_2$ using plasmonic nanodisc arrays," Nano Lett. **15**(4), 2700–2704 (2015).
21. Z. Wang, Z. Dong, Y. Gu, Y.-H. Chang, L. Zhang, L.-J. Li, W. Zhao, G. Eda, W. Zhang, G. Grinblat, S. A. Maier, J. K. W. Yang, C.-W. Qiu, and A. T. S. Wee, "Giant photoluminescence enhancement in tungsten-diselenide-gold plasmonic hybrid structures," Nat. Commun. **7**, 11283 (2016).
22. H. Chen, J. Yang, E. Rusak, J. Straubel, R. Guo, Y. W. Myint, J. Pei, M. Decker, I. Staude, C. Rockstuhl, Y. Lu, Y. S. Kivshar, and D. Neshev, "Manipulation of photoluminescence of two-dimensional MoSe$_2$ by gold nanoantennas," Sci. Rep. **6**(1), 22296 (2016).
23. M. Rycenga, C. M. Cobley, J. Zeng, W. Li, C. H. Moran, Q. Zhang, D. Qin, and Y. Xia, "Controlling the synthesis and assembly of silver nanostructures for plasmonic applications," Chem. Rev. **111**(6), 3669–3712 (2011).
24. J. Kern, A. Trügler, I. Niehues, J. Ewering, R. Schmidt, R. Schneider, S. Najmaei, A. George, J. Zhang, J. Lou, U. Hohenester, S. M. de Vasconcellos, and R. Bratschitsch, "Nanoantenna-Enhanced Light–Matter Interaction in Atomically Thin WS$_2$," ACS Photonics **2**(9), 1260–1265 (2015).
25. K. C. J. Lee, Y.-H. Chen, H.-Y. Lin, C.-C. Cheng, P.-Y. Chen, T.-Y. Wu, M.-H. Shih, K.-H. Wei, L.-J. Li, and C.-W. Chang, "Plasmonic gold nanorods coverage influence on enhancement of the photoluminescence of two-dimensional MoS$_2$ monolayer," Sci. Rep. **5**, 16374 (2015).
26. S. Najmaei, Z. Liu, W. Zhou, X. Zou, G. Shi, S. Lei, B. I. Yakobson, J.-C. Idrobo, P. M. Ajayan, and J. Lou, "Vapour phase growth and grain boundary structure of molybdenum disulphide atomic layers," Nat. Mater. **12**(8), 754–759 (2013).
27. Y.-H. Lee, X.-Q. Zhang, W. Zhang, M.-T. Chang, C.-T. Lin, K.-D. Chang, Y.-C. Yu, J. T.-W. Wang, C.-S. Chang, L.-J. Li, and T.-W. Lin, "Synthesis of Large-Area MoS2 Atomic Layers with Chemical Vapor Deposition," Adv. Mater. **24**(17), 2320–2325 (2012).
28. Y.-H. Lee, L. Yu, H. Wang, W. Fang, X. Ling, Y. Shi, C.-T. Lin, J.-K. Huang, M.-T. Chang, C.-S. Chang, M. Dresselhaus, T. Palacios, L.-J. Li, and J. Kong, "Synthesis and transfer of single-layer transition metal disulfides on diverse surfaces," Nano Lett. **13**(4), 1852–1857 (2013).
29. D. Wang, J.-N. Li, Y. Zhou, D.-H. Xu, X. Xiong, R.-W. Peng, and M. Wang, "Van der Waals epitaxy of ultrathin α-MoO3 sheets on mica substrate with single-unit-cell thickness," Appl. Phys. Lett. **108**(5), 053107 (2016).
30. A. Splendiani, L. Sun, Y. Zhang, T. Li, J. Kim, C. Y. Chim, G. Galli, and F. Wang, "Emerging photoluminescence in monolayer MoS$_2$," Nano Lett. **10**(4), 1271–1275 (2010).
31. J. Jeon, S. K. Jang, S. M. Jeon, G. Yoo, Y. H. Jang, J.-H. Park, and S. Lee, "Layer-controlled CVD growth of large-area two-dimensional MoS$_2$ films," Nanoscale **7**(5), 1688–1695 (2015).
32. J. Zeng, X. Xia, M. Rycenga, P. Henneghan, Q. Li, and Y. Xia, "Successive deposition of silver on silver nanoplates: lateral versus vertical growth," Angew. Chem. Int. Ed. Engl. **50**(1), 244–249 (2011).
33. R. Jin, Y. Cao, C. A. Mirkin, K. L. Kelly, G. C. Schatz, and J. G. Zheng, "Photoinduced conversion of silver nanospheres to nanoprisms," Science **294**(5548), 1901–1903 (2001).
34. C. F. Bohren and D. R. Huffman, *Absorption and Scattering of Light by Small Particles* (Wiley-Interscience, 1983).
35. L. Novotny and B. Hecht, *Principles of Nano-Optics* (Cambridge University Press, 2006).
36. J. A. Schuller, S. Karaveli, T. Schiros, K. He, S. Yang, I. Kymissis, J. Shan, and R. Zia, "Orientation of luminescent excitons in layered nanomaterials," Nat. Nanotechnol. **8**(4), 271–276 (2013).
37. M. Amani, D. H. Lien, D. Kiriya, J. Xiao, A. Azcatl, J. Noh, S. R. Madhvapathy, R. Addou, S. Kc, M. Dubey, K. Cho, R. M. Wallace, S. C. Lee, J. H. He, J. W. Ager 3rd, X. Zhang, E. Yablonovitch, and A. Javey, "Near-unity photoluminescence quantum yield in MoS$_2$," Science **350**(6264), 1065–1068 (2015).
38. S. Mouri, Y. Miyauchi, and K. Matsuda, "Tunable photoluminescence of monolayer MoS$_2$ via chemical doping," Nano Lett. **13**(12), 5944–5948 (2013).
39. X. Gan, Y. Gao, K. Fai Mak, X. Yao, R. J. Shiue, A. van der Zande, M. E. Trusheim, F. Hatami, T. F. Heinz, J. Hone, and D. Englund, "Controlling the spontaneous emission rate of monolayer MoS$_2$ in a photonic crystal nanocavity," Appl. Phys. Lett. **103**(18), 181119 (2013).

40. K. F. Mak, K. He, J. Shan, and T. F. Heinz, "Control of valley polarization in monolayer MoS₂ by optical helicity," Nat. Nanotechnol. **7**(8), 494–498 (2012).

1. Introduction

The remarkable properties of two-dimensional materials allow for emerging research and applications in electronic and optoelectronic area [1, 2]. Transition metal dichalcogenides (TMDCs), such as MoS_2, $MoSe_2$, WS_2 and WSe_2, are layered materials with strong intralayer bonding and weak interlayer adhesion, which enables them to be exfoliated into two-dimensional layer with thickness on the order of a single unit cell [3]. Compared with graphene, MoS_2 has band gap that changes from indirect to direct in monolayer [4], providing significant advantages in optoelectronic applications including photodetectors, sensors, and photovoltaic devices [5–9]. Moreover, the strong spin-orbital splitting at K valley as result of missing inversion symmetry leads to the emerging of valley-based devices [10, 11].

However, in optoelectronics and photonics applications, atomically thin nature of monolayer thickness poses a challenge due to the weak light-matter interaction [12]. The reported experimental results have shown that both light absorbance and emission are weak in monolayer MoS_2 slab [5, 13]. Given this inherent limitation in the atomically thin slab, optical antennas can be used to boost the light-matter interaction [14–17]. They can convert freely propagating electromagnetic wave into localized field, typically on nanometer scale [18], which is compatible with the thickness of monolayer MoS_2. On the other hand, they can also serve as transmitters to direct the radiative wave, thus significantly improving the emission efficiency. Nanostructures of noble metals can serve as antennas in the visible range due to the collective oscillation of electrons in the conduction band in resonance with optical field. Researchers have reported the enhanced spontaneous emission by lithographically defined nanostructures [19, 20], among which a giant effective enhancement up to ~20,000-fold has been achieved by transferring WSe_2 onto gold trenches [21]. Simulation work regarding the gap-dependent emission enhancement in another TMDC $MoSe_2$ has also been reported [22]. In our study, we use solution-processable silver platelet antennas among all types of metallic nanostructures due to their polarization-independent resonance in the range of interest [23]. We report on boosting the light-matter interaction in monolayer MoS_2 by leveraging single crystalline ultrathin antennas to control both excitation and emission processes. These antennas have large potential to improve the quantum yield of nearby emitters at nanoscale [15]. Emission enhancement up to 6-fold in TMDC with drop-casted asymmetric gold nanorods has been experimentally demonstrated [24, 25]. Here we have achieved the polarization-insensitive emission enhancement in platelet antenna-MoS_2 hybrid system by both experiment and simulating the optical processes involved.

2. Methods

2.1 Preparation of monolayer MoS₂ and platelet antennas

Monolayer MoS_2 flakes is synthesized using chemical vapor deposition (CVD) method with a double-temperature-zone furnace [26–29]. High pure sulfur powder (99.9% Alfa Aesar) and MoO_3 powders (99.9% Alfa Aesar) are used as initial reactants, and polished silicon substrate (100) with 300 nm thermal oxide layer is used as the epitaxy substrate. The growth temperature is kept at 800 °C with Ar flow of 100 standard cubic centimeter per minute (sccm) at ambient pressure. MoS_2 triangular flakes with size of around 20 μm are obtained after 20 minutes. The thickness and morphology of MoS_2 is confirmed by using atomic force microscopy (AFM) working under tapping mode as shown in Fig. 1(a).

Micro-photoluminescence (PL) measurements are conducted at room temperature using a confocal Raman microscope equipped with a solid-state laser diode. An objective lens with large numerical aperture (NA = 0.9) is used for optical measurement, so that most of the radiated power can be collected by the objective lens. In the setup, the laser spot size is around 1 μm² when NA is 0.9. 532 nm pump laser is used since it is away from the emission

wavelength of the excitons in monolayer MoS_2 [13]. The PL spectrum is shown in Fig. 1(b). The strong peak at 680 nm and the small peak at 635 nm correspond to A exciton and B exciton respectively, which result from spin-orbital splitting at the valence band maximum [30]. The absence of indirect transition from the bulk value of 1.3 eV (~954 nm) to around 1.6 eV (~775 nm) in PL curve is an indicator of monolayer MoS_2 [13]. In the Raman spectrum in Fig. 1(c), E_{2g} mode (387 cm^{-1}) corresponds to in-plane lattice vibration, while A_{1g} mode (408 cm^{-1}) corresponds to out-of-plane vibration. The peak around 525cm^{-1} comes from the silicon substrate. The frequency difference 21 cm^{-1} between E_{2g} and A_{1g} modes is another indicator of the monolayer nature [31].
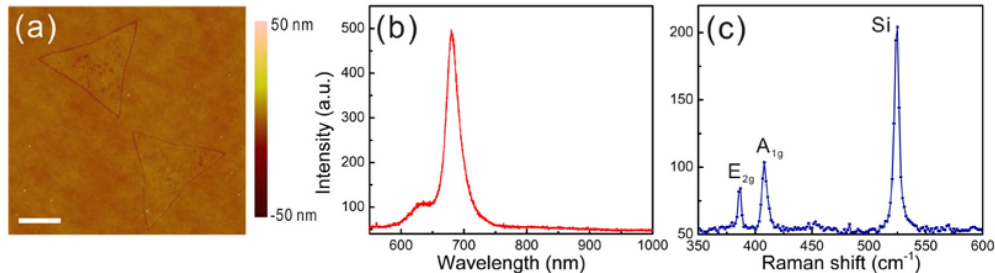

Fig. 1. Characterization of monolayer MoS_2. (a) AFM image of MoS_2 flakes grown by CVD (scale bar: 10 μm). (b) Photoluminescence spectra of as-prepared monolayer MoS_2. (c) Raman spectra of as-prepared monolayer MoS_2. The peaks at 387 cm^{-1} and 408 cm^{-1} correspond to in-plane and out-of-plane lattice vibration, respectively. The peak around 525cm^{-1} comes from the silicon substrate.

Ultrathin silver nanoplates are obtained using a seed-mediated growth method [32]. The size of the nanoplates, and therefore the resonance peak, can be tuned by the number of growth cycles. In the synthesis process, two steps are involved. In the first step, a suspension of spherical seeds is prepared by reducing silver nitrate solution with sodium borohydride. After the solution has been aged for 5 hours, it is mixed with capping agent trisodium citrate, stabilizer polyvinylpyrrolidone and a milder reducing agent L-ascorbic acid. Then the solution is treated by centrifugation to remove the excessive polymer and is concentrated for future use. The nanoplates can be grown further if we repeat the second step [32]. The size of the nanoplate is sensitive to the recipe in the synthesis process. The extinction curve in Fig. 2(b) measured by UV-Vis spectroscopy shows that the plasmon resonance of the silver platelet antennas in the water is between 740 and 760 nm. The peak at around 400 nm is due to the presence of a small number of spherical particles [33]. The shape and size of the platelet antennas are characterized by high-resolution transmission electron microscope (HRTEM), and shown in Fig. 2(a). The inset Figure corresponds to the side view of the platelet antennas. It is obtained when the solution is concentrated and dried down onto the TEM grid. These Figures verify the antenna has circular disc shape with diameter of around 80 nm and thickness of about 6 nm. The Mie scattering cross-section of a single platelet antenna on a SiO_2/Si substrate in Fig. 2(c) is calculated by finite-difference time-domain (FDTD) simulation [34]. The resonance of the antennas will red shift due to the presence of the substrate or supporting material. There is some overlap between the spectrum of antenna resonance and PL of MoS_2 in Fig. 2(c), which indicates that the optical processes in MoS_2 can be controlled by the antenna.
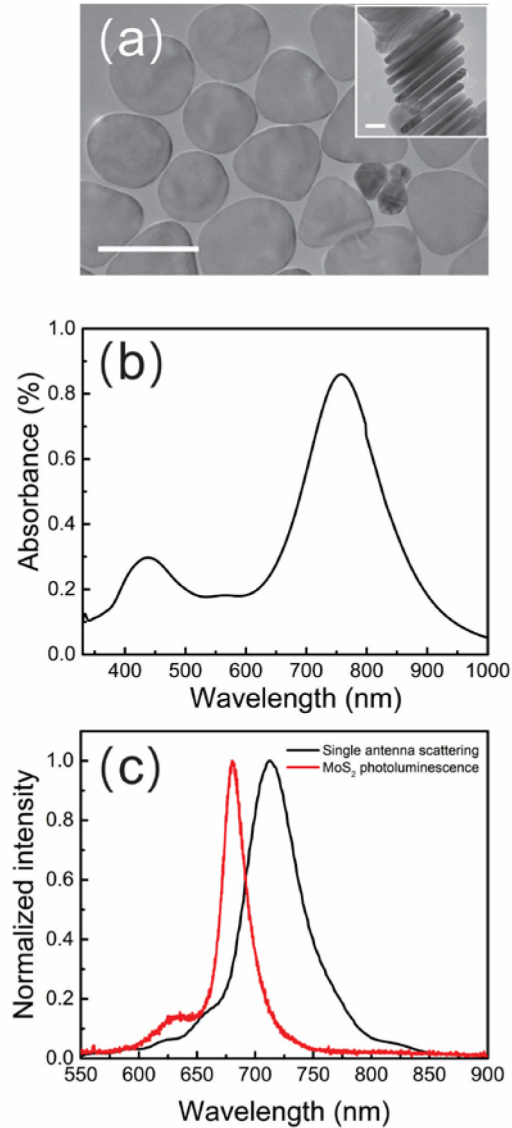
Fig. 2. Plasmon resonance of silver platelet antennas. (a) Shape and size of the platelet antennas characterized by HRTEM. Scale bar: 100 nm. (Inset: side view. Scale bar: 20 nm.) (b) Absorbance of the colloidal silver platelet antenna solution measured by UV-Vis spectroscopy. (c) Antenna resonance on SiO_2/Si substrate calculated by FDTD simulation and MoS_2 photoluminescence.

2.2 Theoretical formulation

Figure 3(a) shows a schematic representation of the MoS_2/antennas heterostructure including MoS_2/SiO_2/Si layers. Since the antennas are randomly distributed, the coupling effect among them is ignored. Perfectly matched layer (PML) boundary condition is used in the FDTD simulation. The antenna can affect both light absorption and emission of MoS_2. The resulting PL enhancement is expressed as [35]

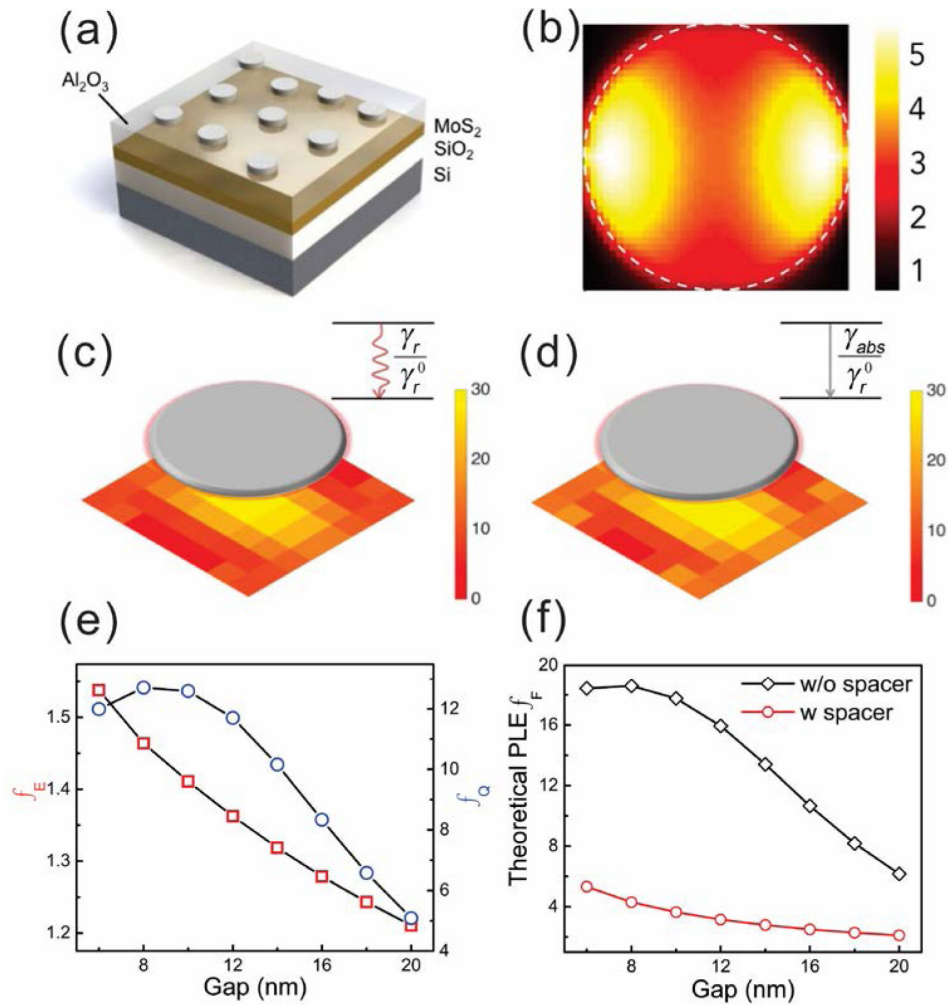$$f_F = f_E f_Q = \frac{\gamma_{exc}}{\gamma_{exc}^0} \frac{q}{q^0} \tag{1}$$

Fig. 3. Simulated spontaneous emission enhancement of MoS_2. (a) Schematic view of the antennas/MoS_2/SiO_2/Si heterostructure. (b) Simulated excitation rate enhancement f_E (gap = 12 nm). (c) Simulated radiative rate enhancement γ_r / γ_r^0 and (d) nonradiative rate enhancement $\gamma_{abs} / \gamma_r^0$ (gap = 12 nm). (e) Field enhancement f_E (red square) and quantum yield enhancement f_Q (blue circle) with respect to the gap thickness. (f) Theoretical PL enhancement (PLE) f_F with (red line) and without (black line) spacer layer.

where γ_{exc} is the excitation rate and q is the quantum yield in the presence of the antenna. The superscript '0' denotes the quantities in the absence of the antenna. f_E and f_Q represent excitation rate enhancement and quantum yield enhancement, respectively. The theoretical PL enhancement is obtained by FDTD simulation. The excitation rate enhancement, also known as field enhancement, is [15, 17]

$$f_E = \frac{\gamma_{exc}}{\gamma_{exc}^0} = \frac{\left| \vec{E}_{exc} \cdot \hat{n}_p \right|^2}{\left| \vec{E}_{exc}^0 \cdot \hat{n}_p \right|^2} \tag{2}$$

where $\vec{E}_{exc}$ represents the excitation field, which is the sum of the total incident plus scattered field, and $\hat{n}_p$ is the unit vector of the emitter. The orientation of emission center of monolayer MoS_2 is in-plane [36] and therefore the total field along z axis will not excite MoS_2. MoS_2 is represented by a horizontal dipole, so both the field enhancement and quantum yield enhancement are averaged over different locations due to the finite size of the platelet antenna. Electric field profiles for different gap distance are simulated in order to obtain the field enhancement. In Fig. 3(b), a representative profile of total electric field intensity under 532 nm excitation at a distance of 12 nm from the antenna is demonstrated. This off-resonance excitation process agrees with the experimental scenario in which a 532 nm laser is used. In the next step, we calculate the enhancement of quantum yield, which is defined as the fraction of radiative decay among all the possible decay channels, by obtaining the radiative and nonradiative decay rate enhancement respectively in Fig. 3(c) and (d). In the absence of antenna, the quantum yield, i.e. $q^0 = \gamma_r^0 / (\gamma_r^0 + \gamma_{nr}^0)$, is an intrinsic property independent of the interaction between the quantum system and the environment. γ_r^0 represents the intrinsic radiative decay rate while γ_{nr}^0 represents the intrinsic nonradiative decay rate. The low intrinsic quantum yield of MoS_2, typically on the order of 10^{-3}, is mainly due to the defect-mediated nonradiative decay [37]. When the antenna is present, the total spontaneous emission rate of a dipole can be represented as:

$$\gamma_{sp} = \gamma_r + \gamma_{abs} + \gamma_{nr}^0 = \frac{\pi\omega}{3\hbar\varepsilon_0}\left|\vec{p}\right|^2 \rho(\vec{r},\omega) + \gamma_{nr}^0 \tag{3}$$

which is the sum of the radiative decay rate γ_r, absorption-induced nonradiative decay rate γ_{abs} and the intrinsic nonradiative decay rate γ_{nr}^0 of the emitter. The radiative and nonradiative decay rates are determined by the dipole moment $\vec{p}$ and the nearby photonic density of states $\rho(\vec{r},\omega)$, in which ω is the oscillation frequency of the dipole. The quantum yield enhancement induced by the antenna can be obtained by calculating the contribution of different decay channels. We can then express the modified quantum yield as $q = \gamma_{rad} / \gamma_{sp}$, and the resulting quantum yield enhancement is:

$$f_Q = \frac{q}{q^0} = \frac{\dfrac{\gamma_r}{\gamma_r^0}}{\left(\dfrac{\gamma_r}{\gamma_r^0} + \dfrac{\gamma_{abs}}{\gamma_r^0}\right)q^0 + (1-q^0)} \tag{4}$$

In the equation above, the radiative and nonradiative decay rate enhancement can be obtained by calculating the power transfer in the emission process based on the relationships $\gamma_r / \gamma_r^0 = P_r / P_r^0$ and $\gamma_{abs} / \gamma_r^0 = P_{abs} / P_r^0$. In the simulation, a dipole source is placed in the gap region. The enhancement factors are obtained by normalizing the radiative power P_r into free space and the power dissipated into the antenna P_{abs} to the radiative power P_r^0 in the absence of the antenna. Figure 3(c) and (d) show the radiative and nonradiative decay rate enhancement at different locations in the gap region, respectively. Here we only show the simulation results when the gap is 12 nm for demonstration purpose. In this particular case, the antenna efficiency is around 50%. The slightly higher nonradiative decay rate indicates the absorption-dominant resonance of the antenna [35], which arises from the ultrathin nature of the platelet antenna. The average quantum yield enhancement in Fig. 3(e) reaches maximum when the dipole-antenna distance is around 8 nm. The smaller quantum yield enhancement at sufficiently small gap arises from the dominance of nonradiative decay. This

decay channel weakens when the gap reaches 8 nm. The gap-dependent quantum yield enhancement curve indicates the competition between rate enhancement and gap increase. The joint effects of excitation and emission enhancement can result in around 18 times enhancement in the total spontaneous emission as indicated by the black curve in Fig. 3(f). The red curve in Fig. 3(f) shows the theoretical PL enhancement with Al_2O_3 as spacer layer, which plays an important role in the real fabrication process.
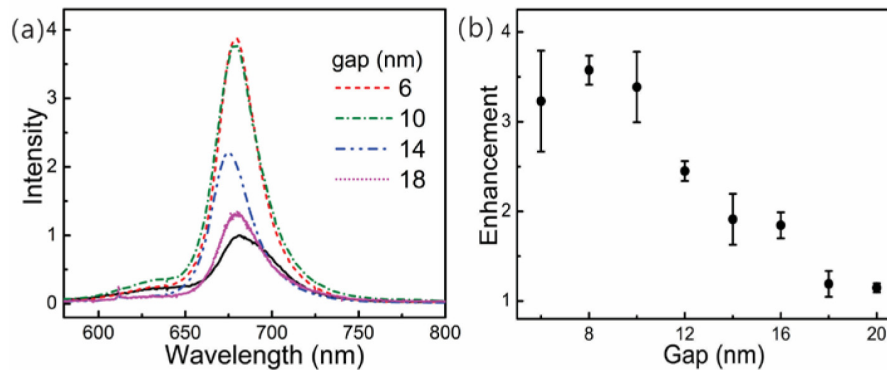
3. Experimental verifications

Fig. 4. Experimental demonstration of emission enhancement from monolayer MoS_2. (a) PL spectra normalized to antenna-free sample (solid black line) at spacer thickness: 6 nm, 10 nm, 14 nm and 18 nm, respectively. (b) PL enhancement factor f_F with respect to the thickness of spacer layer. Standard deviation of three measurements is used for error bars in the Figure.

We then experimentally verify the PL enhancement factor f_F with respect to the change of gap thickness. Aluminum oxide (Al_2O_3) is deposited on MoS_2 by atomic layer deposition (ALD). Precursors are trimethyl aluminum (TMA) and H_2O, while the thickness of Al_2O_3 is controlled by the number of deposition cycles. The presence of Al_2O_3 affects both the excitation and emission of MoS_2 because of the change in the surrounding refractive index. As reference, micro-PL measurements are conducted on the Al_2O_3-covered samples when antennas are absent. The asymmetric shape of the black spectrum different from Fig. 2(b) may arise from trion (A^-) emission at around 700 nm, which could be enhanced after the deposition of Al_2O_3 layer due to n-type doping [38]. After that, 10 μL droplet of platelet antenna solution is drop-casted onto them, and the samples are washed with deionized water and blow-dried with nitrogen gas to minimize the possible formation of clusters. For all the samples, we have chosen a solution concentration at which there are a fair number of antennas within 1 μm² laser spot area. In this way, multiple antennas are excited at the same time. Since the antennas prepared by colloidal method are randomly distributed, here we have not considered the coupling effect among them. The measurement of PL curves can be seen in Fig. 4(a). For each sample, the measured PL intensity is normalized to the peak intensity when there is no antenna. The total PL enhancement factor is 3.9, 3.8, 2.2 and 1.4 when the gap thickness is 6 nm, 10 nm, 14 nm and 18 nm, respectively. The enhancement effect almost vanishes when the gap is larger than 18 nm. Because the PL intensity may vary across the MoS_2 flake, three PL measurements for each sample are taken by probing the laser spot at different locations on MoS_2 flake. The average enhancement factor calculated from three measurements in Fig. 4(b) shows good agreement with the simulated red line in Fig. 3(f) both in the trend and magnitude. The discrepancy between simulation and experiment may be attributed to the inhomogeneous distribution of antennas on MoS_2 flake, and the photon collection efficiency of the experimental setup. More rigorous theoretical analysis might be

needed for small gap thickness. The small shift in PL peak position results from the mismatch between antenna resonance and MoS_2 emission, as well as the size inhomogeneity of antennas on different samples. The presence of spacer layer can modify both excitation rate and quantum yield enhancement by changing the surrounding refractive index [35]. Furthermore, spacer layer will also affect the emission pattern. A higher PL enhancement may be possible if we replace Al_2O_3 with a low index material.

4. Conclusion

In conclusion, we have demonstrated ultrathin antenna-enhanced spontaneous emission from the low-quantum-yield 2D semiconductor MoS_2. The enhancement factor can be around 4 times as shown in the experiments. We also estimate the theoretical enhancement factor by simulating both excitation and emission processes. The gap-dependent PL enhancement shows qualitative agreement with simulation both in the trend and magnitude. Compared with using lithographically fabricated antennas, the solution-processable nature of our method can be more effective in cases of large area sample and flexible substrate. We can expect high quantum yield without transferring MoS_2 onto other substrates, such as photonic crystal [39] and hBN flakes [40]. Moreover, this antenna-coupled system has short emission lifetime and can thus transfer energy more efficiently. It is anticipated that the ultrathin platelet antennas together with monolayer MoS_2 hold promise for the development of on-chip emitters and valley-based devices.